

Topology optimization for designing strain-gauge load cells

A. Takezawa · S. Nishiwaki · M. Kitamura · Emilio C. N. Silva

Received: date / Accepted: date

Abstract Load cells are used extensively in engineering fields. This paper describes a novel structural optimization method for single- and multi-axis load cell structures. First, we briefly explain the topology optimization method that uses the solid isotropic material with penalization (SIMP) method. Next, we clarify the mechanical requirements and design specifications of the single- and multi-axis load cell structures, which are formulated as an objective function. In the case of multi-axis load cell structures, a methodology based on singular value decomposition is used. The sensitivities of the objective function with respect to the design variables are then formulated. On the basis of these formulations, an optimization algorithm is constructed using finite element methods and the method of moving asymptotes (MMA). Finally, we examine the

characteristics of the optimization formulations and the resultant optimal configurations. We confirm the usefulness of our proposed methodology for the optimization of single- and multi-axis load cell structures.

Keywords Load cell · Topology optimization · Singular value decomposition · Compliant mechanism · Strain gauge

1 Introduction

Load cells are used extensively in engineering fields. For example, simple single-axis sensors called “load cells” are used to measure applied forces in various experiments. In automotive development, six-axis force transducers are required when measuring the values of the force components applied to wheels (Weiblen and Hofmann, 1998). These multi-axis load cells are also used in robotic manipulators in factory automation engineering (Kaneko, 1996; Kim and Lee, 2003; Uchiyama et al., 1991b; Park and Kim, 2005), with sensors composed of sensing devices such as strain gauges and force transducer structures. The transducer structures convert the forces applied to the sensor’s measuring point into strains that are then detected by the sensing devices. In cases where strain gauges are used as sensing devices, strain values are transformed to resistance variations in the device. These are ultimately detected as output voltage fluctuations using a Wheatstone bridge, which are used to calculate each component of the applied force. If there is one detected force component, the load cell is called a single-axis sensor. If there are more than one, the device is called a multi-axis sensor.

The performance of such load cells can be evaluated according to criteria such as the static and dynamic stiffness of the sensor structures, weight, force detection

A. Takezawa · M. Kitamura
Department of Social and Environmental Engineering
Graduate School of Engineering, Hiroshima University,
1-4-1 Kagamiyama, Higashi-hiroshima, Hiroshima 739-8527,
Japan
Tel.: +81-82-424-7544
Fax: +81-82-422-7194
E-mail: akihiro@hiroshima-u.ac.jp

S. Nishiwaki
Department of Mechanical Engineering and Science
Graduate School of Engineering, Kyoto University,
Sakyo-ku, Kyoto 606-8501, Japan
E-mail: shinji@prec.kyoto-u.ac.jp

M. Kitamura
E-mail: kitamura@hiroshima-u.ac.jp

Emílio C. N. Silva
Department of Mechatronics and Mechanical
Systems Engineering,
Escola Politécnica da Universidade de São Paulo,
Av. Prof. Mello Moraes, 2231, São Paulo,
SP 05508-900, Brazil
E-mail: ecnsilva@usp.br

sensitivity and accuracy. In the case of single-axis load cells, the function is quite simple and only sensitivity and stiffness need to be considered. However, in addition to these criteria, in the case of a multi-axis load cell, the detection accuracy of each force component is invariably considered the most important parameter for evaluating the sensor performance. If the force detection errors caused by strain sensing errors are quite different at each force component, the errors are hard to calibrate out. Thus, differences in the detection accuracies of each component of the applied force should be small. One well-known method for evaluating such sensor performance is based on singular value decomposition (SVD) (Uchiyama et al., 1991b) and it represents the performance as a condition number of a transforming matrix that expresses the relationship between the applied forces and the measured strains.

Although the theory, which is based on SVD, is clear and has a well-developed mathematical foundation based on linear algebra, it is difficult to apply the methodology to the structural design of transducers. The theory is generally expressed in terms of control system performance, which provides little insight into the basic mechanics of the target structures. Thus, the theory is hard to apply to ordinary mechanical design. To achieve a mechanical design based on the theory, a number of numerical structural optimization methods have been proposed (Bayo and Stubbe, 1989; Chao and Chen, 1997; Kim et al., 2002; Uchiyama et al., 1991a; Liu and Tzo, 2002), however these methodologies are based on size or shape optimizations and thus strongly depend on the quality of initial structural design, with the result that novel high performance structural design remains elusive.

On the other hand, topology optimization methods have been extensively applied to a variety of structural optimization problems (Bendsøe and Sigmund, 2003) since Bendsøe and Kikuchi first proposed a so-called homogenization design method (HDM) (Bendsøe and Kikuchi, 1988). This method offers the greatest potential for exploring ideal and optimized structures because it allows changes in topology as well as shape. The basic concept consists of the extension of a design domain to a fixed design domain, and the replacement of the optimization problem with a material distribution problem. These ideas introduce the holes nucleation mechanism which is not achieved by the classical shape optimization based on boundary variation. Since the optimization problem has extreme discontinuity, there are no optimal solutions to the problem (Allaire, 2001). A homogenization method is used to deal with the extreme discontinuity in the material distribution and to provide material properties viewed, in

a global sense, as homogenized properties. This method and its variant solid isotropic material with penalization (SIMP) method (Bendsøe, 1989; Bendsøe and Sigmund, 1999; Zhou and Rozvany, 1991) has been applied to a variety of design problems. Beginning with the optimization for structural stability such as the stiffness maximization and eigenfrequency maximization problem (Bendsøe and Kikuchi, 1988; Krog and Olhoff, 1999; Ma et al., 1995; Pedersen, 2000; Suzuki and Kikuchi, 1991), topology optimization is extended to the actuator mechanism design problem (Canfield and Frecker, 2000; Nishiwaki et al., 1998; Sigmund, 1997, 2001; Silva et al., 2000). We focus on piezoelectric actuator design problems (Canfield and Frecker, 2000; Silva et al., 2000). The underlying concept in these methods is maximization of the displacement of the output point caused by an input strain on the piezoelectric device. The opposite optimization problem, the maximization of strain at a specified point caused by an applied load, can be regarded as a sensor design problem if some sensor devices are located on the specified point. Some topology optimization methods for sensor structure have been reported. Pedersen (Pedersen, 2004) and Rubio et al. (Rubio et al., 2008) proposed an optimization method for the piezoresistive load cell. However, the topology optimization for multi-axis load cells has not been reported.

In this paper, we develop a novel topology optimization method for conceptual designs of basic single- and multi-axis load cell structures whose sensor devices are strain gauges. First, we briefly explain the topology optimization method that uses the solid isotropic material with penalization (SIMP) method. Next, we clarify the mechanical requirements and design specifications of each sensor structure. In the case of a multi-axis load cell, this is based on the SVD. We formulate the objective functions for each sensor and construct an optimization problem that aims to satisfy the design specifications. Sensitivities of the objective functions with respect to the design variables that are required in the optimization procedure are formulated. Based on these formulations, an optimization algorithm is constructed using the finite element method (FEM) and the method of moving asymptotes (MMA) (Svanberg, 1987). Finally, we examine the characteristics of the optimization formulations and the generated optimal configurations, and confirm the usefulness of our proposed methodology for the optimization of single- and multi-axis load cell structures.

2 Formulation

2.1 Topology optimization

When considering the design problem of determining the design domain Ω_d to minimize objective functions, the key idea of topology optimization is to introduce a fixed, extended design domain D that includes, a priori, the original design domain Ω_d and the utilization of the following characteristic function:

$$\chi(\mathbf{x}) = \begin{cases} 1 & \text{if } \mathbf{x} \in \Omega_d \\ 0 & \text{if } \mathbf{x} \in D \setminus \Omega_d \end{cases} \quad (1)$$

where \mathbf{x} denotes a position in the extended design domain D . Using this function, the original structural design problem is replaced by a material distribution problem incorporating an elasticity tensor, $\chi\mathbf{A}$, in the extended design domain D , where \mathbf{A} is the elasticity tensor in the original design domain Ω_d . Since this characteristic function can be discontinuous, i.e. resides in $L^\infty(D)$, some regularization techniques should be introduced. A homogenization method is used to perform the relaxation of the solution space (Bendsøe and Kikuchi, 1988; Allaire, 2001). In this way, with respect to the characteristic function, the original material distribution optimization problem is replaced by an optimization problem of a “composite” made up of the original material and a very weak material that imitates the void, using a density function. The density function represents the volume fraction of the original material and can be regarded as a weak limit of the characteristic function. In the optimization problem, the relationship between the material properties of the composite and the density function must be defined. Several approaches have been proposed for this. One was to define a simple microstructure, calculate the material property using the asymptotic method (Bendsøe and Kikuchi, 1988; Suzuki and Kikuchi, 1991; Matsui and Terada, 2004), and set a completely artificial material property (Bendsøe, 1989; Bendsøe and Sigmund, 1999; Zhou and Rozvany, 1991). Another approach is called the solid isotropic material with penalization (SIMP) method, which is a popular method used in topology optimization. In this method, the material property is defined in the following simple equation that includes a penalized material density function.

$$\mathbf{A}^* = \rho^p \mathbf{A} \quad (2)$$

where \mathbf{A}^* is the material property of the composite, ρ is the density function representing the volume fraction of the original material and p is a positive penalization parameter. This method has the advantage of controlling the non-linearity between the material property of

the composite and the density function, which has a significant role in avoiding “gray” regions where assessing the presence of material or void is problematic. The SIMP method is used in this research.

Topology optimization methods can also encounter a numerical instability problem that causes checkerboard patterns (Diaz and Sigmund, 1995; Sigmund and Petersson, 1998) depending on settings. To mitigate this problem, so-called filtering techniques are introduced (see (Sigmund, 2007) and references therein). In this research, filtering is implemented based on the projection method (Guest et al., 2004). This method sets design variables in addition to the density function and “projects” these design variables onto the density function using a projection function. By adjusting the effective range and shape of the function, checkerboard patterns can be avoided. First, a weighted average function using a simple linear projection function is considered, as follows:

$$\mu(d(\mathbf{x}_e)) = \frac{\int_{\Omega_e} dw(\mathbf{x} - \mathbf{x}_e)dx}{\int_{\Omega_e} w(\mathbf{x} - \mathbf{x}_e)dx} \quad (3)$$

where:

$$\Omega_e(\mathbf{x}_e) = \{\mathbf{x} \mid \|\mathbf{x} - \mathbf{x}_e\| \leq r_{\min}, \mathbf{x} \in D\} \quad (4)$$

where Ω_e is the circular effective area of the projection function of design variable d at \mathbf{x}_e , d is the design variable function, r_{\min} is the radius of the effective area of the projection function and w is the following linear weighting function:

$$w(\mathbf{x} - \mathbf{x}_e) = \begin{cases} \frac{r_{\min} - \|\mathbf{x} - \mathbf{x}_e\|}{r_{\min}} & \text{if } \mathbf{x} \in \Omega_e \\ 0 & \text{if } \mathbf{x} \in D \setminus \Omega_e \end{cases} \quad (5)$$

To obtain solutions that closely approach either 0 or 1 from the above average volume fraction, the final volume fraction is calculated using a smoothed Heaviside step function as follows:

$$\rho(\mathbf{x}_e) = 1 - e^{-\beta\mu(d(\mathbf{x}_e))} + \mu(d(\mathbf{x}_e))e^{-\beta} \quad (6)$$

The above functions are calculated numerically by appropriate discretization. In the original paper (Guest et al., 2004), the discretized design variable function was set to the nodes of the finite element mesh. However, in this research, we discretize the function at the center of each element to simplify the sensitivity calculations.

2.2 Objective function for single-axis load cell

First, the objective function for a single-axis load cell that will measure an applied force in a specified direction is formulated. Loadcell sensitivity to applied loads and stiffness against these loads are key design requirements for single-axis load cells. Here, we focus on the sensitivity maximization problem as the main optimization target. The output voltage caused by applied loads at a specified load point is used as an index of the sensitivity of the sensors. We consider the case in which a load is applied to a 2-D domain Ω_e composed of elastic material with strain gauges n_g located in the domain at position \mathbf{x}_g , to detect the strain caused by the applied force. For simplicity and consistency with the multi-axis load cell problem to be described later, the domain is discretized using the finite element method, and the load is assumed to be a point load. The resistance variation of the i_g -th strain gauge is formulated as follows:

$$\frac{\Delta R_{i_g}}{R_{i_g}} = K_s \varepsilon_g(\mathbf{x}_{g_{i_g}}) \quad (7)$$

where ε_g is the strain detected by the strain gauge, that is, an x -component of the strain with respect to the local coordinate of the strain gauges shown in Fig.1. K_s is a gauge factor. ε_g is calculated based on the strain $\boldsymbol{\varepsilon}$ with respect to the global coordinate system as follows:

$$\varepsilon_g(\mathbf{x}_{g_{i_g}}) = \mathbf{T}_{i_g} \boldsymbol{\varepsilon}(\mathbf{x}_{g_{i_g}}) \quad (8)$$

where \mathbf{T}_{i_g} is a matrix connecting $\varepsilon_{g_{i_g}}$ and $\boldsymbol{\varepsilon}_{i_e}$ formulated as follows:

$$\mathbf{T}_{i_g} = \begin{pmatrix} \cos^2 \theta & \sin^2 \theta & 2 \sin \theta \cos \theta \end{pmatrix} \quad (9)$$

In this method, we set the x -direction of the strain gauges to match the direction of the principal strains. Thus, ε_g is obtained as follows:

$$\begin{aligned} \varepsilon_g(\mathbf{x}_{g_{i_g}}) &= \frac{\varepsilon_X(\mathbf{x}_{g_{i_g}}) + \varepsilon_Y(\mathbf{x}_{g_{i_g}})}{2} \\ &\pm \sqrt{\left(\frac{\varepsilon_X(\mathbf{x}_{g_{i_g}}) - \varepsilon_Y(\mathbf{x}_{g_{i_g}})}{2} \right)^2 + \gamma_{XY}(\mathbf{x}_{g_{i_g}})^2} \end{aligned} \quad (10)$$

where ε_X , ε_Y and γ_{XY} are strain and shear strain components with respect to global coordinate systems.

The resistance variations of these strain gauges are detected as variations of the output voltage of the Wheatstone bridge composed of these strain gauges. Since a Wheatstone bridge is composed of up to four strain

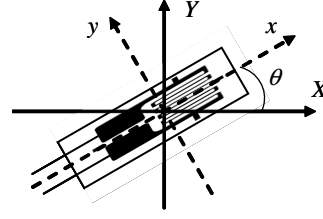


Fig. 1 Coordinate system of strain gauge

gauges, using the values of the detected strains, the output voltage V_{out} of the Wheatstone bridge is obtained as follows:

$$\begin{aligned} V_{\text{out}} &= \frac{1}{4} V_{\text{in}} \left(\frac{\Delta R_1}{R_1} - \frac{\Delta R_2}{R_2} + \frac{\Delta R_3}{R_3} - \frac{\Delta R_4}{R_4} \right) \\ &= \frac{1}{4} K_s V_{\text{in}} (\varepsilon_g(\mathbf{x}_{g_1}) - \varepsilon_g(\mathbf{x}_{g_2}) + \varepsilon_g(\mathbf{x}_{g_3}) - \varepsilon_g(\mathbf{x}_{g_4})) \end{aligned} \quad (11)$$

where V_{in} is the input voltage of the Wheatstone bridge. The maximum value of V_{out} is obtained if the signs of ε_g are $\varepsilon_g(\mathbf{x}_{g_1}) \geq 0$, $\varepsilon_g(\mathbf{x}_{g_3}) \geq 0$ and $\varepsilon_g(\mathbf{x}_{g_2}) \leq 0$, $\varepsilon_g(\mathbf{x}_{g_4}) \leq 0$. However, these conditions cannot always be satisfied. Thus, in this method, we use the following virtual output voltage during the optimization process:

$$V_{\text{out}} = \frac{1}{4} K_s V_{\text{in}} \sum_{i_g=1}^{n_g} |\varepsilon_g(\mathbf{x}_{i_g})| \quad (12)$$

where $n_g \leq 4$ is the number of strain gauges used in the Wheatstone bridge. The signs of the strains are not always the ideal case, for example two of them may be positive and the others negative. According to the signs of strains, more than one Wheatstone bridge can be constructed. For example, if two values of $\Delta R/R$ are positive and the others are negative as shown in Fig.2(a), the resistance variations of all strain gauges can be detected using only one Wheatstone bridge, and the output voltage of the circuit is as is shown in Eq.(11). Even if the signs of resistance variations are not ideal, as in Fig.2(b), the output voltage including all resistance variations can be obtained by constructing two Wheatstone bridges as follows:

$$\begin{aligned} V_{\text{out}} &= \frac{1}{4} V_{\text{in}} \left(\frac{\Delta R_1}{R_1} + \frac{\Delta R_2}{R_2} \right) + \frac{1}{4} V_{\text{in}} \left(\frac{\Delta R_3}{R_3} + \frac{\Delta R_4}{R_4} \right) \\ &= \frac{1}{4} V_{\text{in}} \left(\frac{\Delta R_1}{R_1} + \frac{\Delta R_2}{R_2} + \frac{\Delta R_3}{R_3} + \frac{\Delta R_4}{R_4} \right) \end{aligned} \quad (13)$$

The maximization of the above total output voltage of the Wheatstone bridges can be obtained by maximizing the structural flexibility. However, if only structural

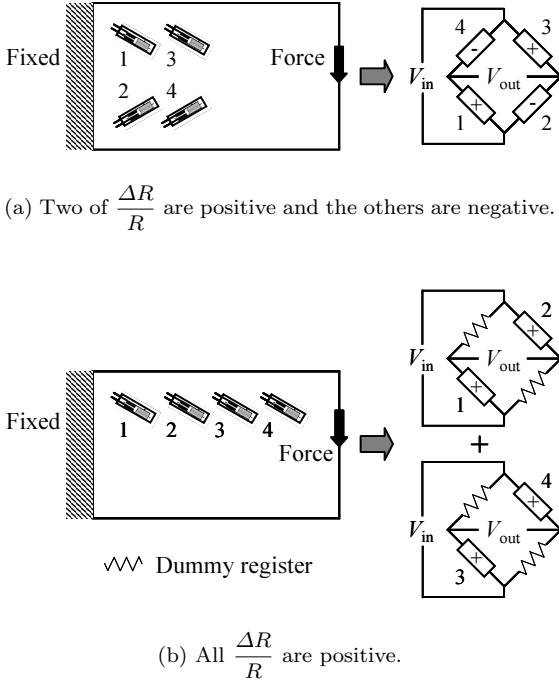


Fig. 2 Construction examples of Wheatstone bridges

flexibility maximization is considered, the optimal configuration will have insufficient stiffness for the applied load and will be hard to implement as an actual sensor structure. To obtain optimal structures with a certain level of stiffness for the applied forces, we add the following mean compliance l into the objective function:

$$l = \mathbf{F}^T \mathbf{U} \quad (14)$$

where \mathbf{F} and \mathbf{U} are the discretized load and displacement vectors, respectively. Finally, the objective function for a single-axis load cell is obtained as the weighted summation of Eq.(12) and Eq.(14) as follows:

$$f_{\text{single}} = -w_V V_{\text{out}} + w_l l \quad (15)$$

where

$$w_V + w_l = 1 \quad (16)$$

where w_V and w_l are weighting coefficients.

2.3 Objective function for multi-axis load cell

In the design of multi-axis load cells, in addition to the sensitivity and stiffness considered in single-axis load cells, the detection accuracy of each force component needs to be considered when evaluating the sensor performance. Sensing errors are inevitable since the accuracy depends on the strain sensing errors caused by the

strain gauge. Thus, for ideal performance in multi-axis load cells, equal detection accuracies are required for each force component, and any errors should be corrected by calibration. One well-known method for evaluating such sensor performance is based on singular value decomposition (SVD) (Uchiyama et al., 1991b). This method represents the performance as a matrix condition number that expresses the relationship between the applied forces and the measured strains. Based on this method, a new performance index of the multi-axis load cells is introduced to formulate an objective function.

We consider a load cell system for measuring a force with $n \leq 6$ degrees of freedom, and n output signals via the Wheatstone bridges composed of a linear elastic body and strain gauges. Note that it is assumed that the linear elastic problem is represented as a finite dimensional linear system, and here we discretize the linear elastic body using the finite element method. In this research, the 2D problem ($n = 2$) is considered as the simplest case. The relationship between the input force and output signals can be represented as:

$$\mathbf{s} = \mathbf{C}_s \mathbf{f}, \quad \mathbf{C}_s \in \mathbb{R}^{n \times n} \quad (17)$$

where

$$\mathbf{s}^T = (V_{\text{out}1}, \dots, V_{\text{out}n}), \quad \mathbf{s} \in \mathbb{R}^n \quad (18)$$

$$\mathbf{f}^T = (f_1, \dots, f_n), \quad \mathbf{f} \in \mathbb{R}^n \quad (19)$$

where \mathbf{s} is an n -dimensional output signal vector whose components are output voltages of the Wheatstone bridges in Eq.(11), \mathbf{f} is an n -dimensional vector representing the applied force, and \mathbf{C}_s is known as an $n \times n$ matrix or the so-called ‘‘strain compliance matrix’’. \mathbf{C}_s is determined from the location of the strain sensing points, the Wheatstone bridge settings, a load applied point and fixed points. By solving Eq.(17) with respect to \mathbf{f} , the values of the applied force components are obtained. Thus, the performance of the sensor system depends on the matrix \mathbf{C}_s . Certain mathematical techniques are required to evaluate the performance of \mathbf{C}_s . One method for mathematically analyzing \mathbf{C}_s has been proposed in (Uchiyama et al., 1991b) based on the SVD method (Golub and Van Loan, 1996).

The SVD of \mathbf{C}_s is obtained as:

$$\mathbf{C}_s = \mathbf{U}_s \mathbf{\Sigma}_s \mathbf{V}_s^T \quad (20)$$

where

$$\mathbf{\Sigma}_s = \text{diag}(\sigma_1, \dots, \sigma_n) \in \mathbb{R}^{n \times n} \quad (21)$$

$$\mathbf{U}_s = (\mathbf{u}_1, \dots, \mathbf{u}_n) \in \mathbb{R}^{n \times n}, \quad \mathbf{u}_1, \dots, \mathbf{u}_n \in \mathbb{R}^n \quad (22)$$

$$\mathbf{V}_s = (\mathbf{v}_1, \dots, \mathbf{v}_n) \in \mathbb{R}^{n \times n}, \quad \mathbf{v}_1, \dots, \mathbf{v}_n \in \mathbb{R}^n \quad (23)$$

\mathbf{U}_s and \mathbf{V}_s are orthogonal $n \times n$ matrices and $\sigma_1, \dots, \sigma_n$ represent the singular values of \mathbf{C}_s . When the singular values are obtained as:

$$\sigma_1 \geq \dots \geq \sigma_r \geq \sigma_{r+1} = \dots = \sigma_n = 0 \quad (24)$$

the rank of \mathbf{C}_s is defined as:

$$\text{rank}(\mathbf{C}_s) = r \quad (25)$$

Based on the above SVD, the evaluation method for a multi-axis load cell is introduced. As a most fundamental requirement, Eq.(17) must have a unique solution to calculate the applied force based on the output signal. Thus, the rank of \mathbf{C}_s must be equal to its dimension n as follows:

$$\text{rank}(\mathbf{C}_s) = n \quad (26)$$

That is, the following condition can be obtained from Eq.(25):

$$\sigma_n > 0 \quad (27)$$

The second requirement, as for the single-axis load cells, is that the sensitivity of \mathbf{s} with respect to \mathbf{f} should be high, so that the force can be measured with a high degree of accuracy. If $\sigma_n > 0$ is satisfied, the following relationships can be defined (Golub and Van Loan, 1996):

$$\max \frac{\|\mathbf{C}_s \mathbf{f}\|}{\|\mathbf{f}\|} = \max \frac{\|\mathbf{s}\|}{\|\mathbf{f}\|} = \sigma_1 \quad (28)$$

$$\min \frac{\|\mathbf{C}_s \mathbf{f}\|}{\|\mathbf{f}\|} = \min \frac{\|\mathbf{s}\|}{\|\mathbf{f}\|} = \sigma_n \quad (29)$$

where $\|\cdot\|$ represents the Euclidean norm. That is, the relationship between the singular values and norm ratio between \mathbf{s} and \mathbf{f} is can be defined as follows:

$$\sigma_n \leq \frac{\|\mathbf{s}\|}{\|\mathbf{f}\|} \leq \sigma_1 \quad (30)$$

Considering the variation of input force in Eq.(17), $d\mathbf{s} = \mathbf{C}_s d\mathbf{f}$, this can be applied to the variation of \mathbf{s} and \mathbf{f} as follows:

$$\sigma_n \leq \frac{\|d\mathbf{s}\|}{\|d\mathbf{f}\|} \leq \sigma_1 \quad (31)$$

$\|d\mathbf{s}\|/\|d\mathbf{f}\|$ in Eq.(31) can be regarded as the sensitivity of \mathbf{s} with respect to \mathbf{f} . Thus, to increase the sensitivity, its minimum value σ_n should be maximized.

The third requirement is that the errors in the calculations of \mathbf{f} caused by sensing errors in \mathbf{s} should be minimized. If $d\mathbf{s}$ is the sensing error and $d\mathbf{f}$ is the force detection error caused by $d\mathbf{s}$, the following relationship is obtained from Eqs.(30) and (31):

$$\frac{\sigma_n}{\sigma_1} \leq \frac{\|d\mathbf{f}\|/\|\mathbf{f}\|}{\|d\mathbf{s}\|/\|\mathbf{s}\|} \leq \frac{\sigma_1}{\sigma_n} \quad (32)$$

Eq.(32) indicates that the ratio between $\|d\mathbf{f}\|/\|\mathbf{f}\|$ and $\|d\mathbf{s}\|/\|\mathbf{s}\|$ cannot exceed σ_1/σ_n . The force detection error can be minimized by minimizing the ratio between $\|d\mathbf{f}\|/\|\mathbf{f}\|$ and $\|d\mathbf{s}\|/\|\mathbf{s}\|$, i.e., the ratio σ_1/σ_n , the condition number of \mathbf{C}_s , should be minimized. The inverse of Eq.(31), is as follows:

$$\frac{1}{\sigma_1} \leq \frac{\|d\mathbf{f}\|}{\|d\mathbf{s}\|} \leq \frac{1}{\sigma_n} \quad (33)$$

The equation shows the sensitivity range of the force detection error caused by sensing errors. In this equation, we find that minimizing the condition number is equivalent to minimizing the range of the sensitivity. Thus, the operation can also be regarded as an equalization of the detection accuracy of each force component that is equal to the first defined design specification as confirmed in a numerical example.

To satisfy simultaneously the above indices of \mathbf{C}_s , i.e. 1: rank, 2: sensitivity, and 3: detection accuracy of each force component, the following optimization problem is considered:

$$\text{maximize } \sigma_r \quad (34)$$

and

$$\text{minimize } \frac{\sigma_1}{\sigma_r} \quad (35)$$

where

$$\sigma_r > 0 \quad (36)$$

To deal with the above multi-objective optimization problem, we formulate the following equation, using a weighted sum method.

$$\text{minimize } f = -w_s \sigma_r + w_c \frac{\sigma_1}{\sigma_r} \quad (37)$$

where w_s and w_c are the weighting coefficients for the lowest singular value and condition number. The inequality constraints in Eq.(36) are automatically satisfied in the optimization process due to the maximization problem given by Eq.(34) and this can be ignored in Eq.(37).

Adding the compliance term to achieve a certain level of stiffness for the load cell structure as well as the single-axis load cells, an objective function is finally formulated as follows:

$$f_{\text{multi}} = -w_s \sigma_r + w_c \frac{\sigma_1}{\sigma_r} + \sum_{q=1}^m w_{l_q} l_q \quad (38)$$

where

$$w_s + w_c + \sum_{q=1}^m w_l q = 1 \quad (39)$$

where m is the number of considered load cases and w_l are the weighting coefficients for compliances.

2.4 Formulation of optimization problem

We introduced the volume constraint in the optimization problem since the weights of load cell devices are one of the important design factors when they are used in moving devices. Using the objective functions and constraints formulated above, the optimization problem is formulated as follows:

$$\underset{\mathbf{d}}{\text{minimize}} \quad f_{\text{single}} = -w_V V_{\text{out}} + w_l l \quad (40)$$

or

$$\underset{\mathbf{d}}{\text{minimize}} \quad f_{\text{multi}} = -w_s \sigma_r + w_c \frac{\sigma_1}{\sigma_r} + \sum_{q=1}^m w_l q l_q \quad (41)$$

where

$$g(\mathbf{d}) = \sum_{i_e \in D} \rho_{i_e}(\mathbf{d}) v_{i_e} - V^U \leq 0 \quad (42)$$

$$0 \leq d_{i_e} \leq 1 \text{ for } i_e = 1, \dots, n_e \quad (43)$$

$$\mathbf{K}\mathbf{U} = \mathbf{F} \quad (44)$$

where

$$\mathbf{K} = \bigcup_{i_e=1}^{n_e} \mathbf{K}_{i_e} = \bigcup_{i_e=1}^{n_e} \int_{\Omega_{i_e}} \mathbf{B}_{i_e}^T \mathbf{D}_{i_e} \mathbf{B}_{i_e} d\Omega \quad (45)$$

where n_e is the total number of elements, \mathbf{d} is the design variable vector, ρ_{i_e} and v_{i_e} are respectively the discretized density function and original volume of i_e -th element, $g(\mathbf{d})$ is the volume constraint, V^U is the upper volume, \mathbf{U} and \mathbf{F} are respectively the discretized displacement vector and force vector and \mathbf{K} is the stiffness matrix. \mathbf{K}_{i_e} , \mathbf{B}_{i_e} and \mathbf{D}_{i_e} are the element stiffness matrix of i_e -th element, the B-matrix and the elastic matrix, respectively.

3 Numerical Implementation

3.1 Algorithm

The optimization procedure is as follows:

1. Set an initial shape, locate the strain gauges and construct Wheatstone bridges.

2. Iterate the following procedure until convergence.

- (a) Calculate the density function and material properties.
- (b) Calculate the objective function and total volume.
- (c) Calculate sensitivities.
- (d) Based on the sensitivities, update the design variables using the method of moving asymptotes (MMA) (Svanberg, 1987).

3.2 Numerical Implementation for single-axis load cell optimization

3.2.1 Sensitivity analysis

As shown above, in this research, MMA is used to update design variables, and sensitivity analysis is required. We derive the sensitivity for the optimization problem of the single-axis load cell. The sensitivity of the virtual output voltage in Eq.(12) with respect to the density function ρ_{i_e} for element i_e is defined as follows:

$$\frac{\partial V_{\text{out}}}{\partial \rho_{i_e}} = \frac{1}{4} K_s V_{\text{in}} \sum_{i_g=1}^{n_g} \frac{\partial |\varepsilon_{g i_g}^h|}{\partial \rho_{i_e}} \quad (46)$$

The suffix h on the strain represents the discretized value. When the i_g -th strain gauge is located on the center of i_{eg} -th element, $\partial |\varepsilon_{g i_g}^h| / \partial \rho_{i_e}$ is obtained as follows using Eq.(8):

$$\frac{\partial |\varepsilon_{g i_g}^h|}{\partial \rho_{i_e}} = \begin{cases} \mathbf{T}_{i_g} \frac{\partial \varepsilon_{i_{eg}}^h}{\partial \rho_{i_e}} & \text{if } \varepsilon_{g i_g}^h \geq 0 \\ -\mathbf{T}_{i_g} \frac{\partial \varepsilon_{i_{eg}}^h}{\partial \rho_{i_e}} & \text{if } \varepsilon_{g i_g}^h < 0 \end{cases} \quad (47)$$

where $\varepsilon_{i_{eg}}^h$ is the discretized strain of i_{eg} -th element. The function $|\varepsilon_{g i_g}^h|$ is clearly not smooth at $\varepsilon_{g i_g}^h = 0$ and discontinuous weak-sensitivity only exists at this point, however this problem does not affect our practical numerical calculations during the optimization process. The sensitivity of the strain of i_e -th element is obtained as follows:

$$\frac{\partial \varepsilon_{i_{eg}}^h}{\partial \rho_{i_e}} = \mathbf{B}_{i_{eg}} \frac{\partial \mathbf{U}_{i_{eg}}}{\partial \rho_{i_e}} \quad (48)$$

We derive the sensitivity of the strain gauge to displacement of location, $\partial \mathbf{U}_{i_{eg}} / \partial \rho_{i_e}$ by considering the matrix $\mathbf{H}_{i_{eg}}$ connecting the local displacement vector $\mathbf{U}_{i_{eg}}$ and the global displacement vector \mathbf{U} as follows:

$$\mathbf{U}_{i_{eg}} = \mathbf{H}_{i_{eg}}^T \mathbf{U} \quad (49)$$

Using the relationship, $\partial \mathbf{U}_{i_{eg}} / \partial \rho_{i_e}$ is obtained as follows:

$$\frac{\partial \mathbf{U}_{i_{eg}}}{\partial \rho_{i_e}} = \mathbf{H}_{i_{eg}}^T \frac{\partial \mathbf{U}}{\partial \rho_{i_e}} \quad (50)$$

Using the equilibrium equation in Eq.(44), the following equation is obtained:

$$\frac{\partial \mathbf{U}}{\partial \rho_{i_e}} = -\mathbf{K}^{-1} \frac{\partial \mathbf{K}}{\partial \rho_{i_e}} \mathbf{U} \quad (51)$$

The sensitivity of the local displacement of the i_e -th element is as follows:

$$\frac{\partial \mathbf{U}_{i_{eg}}}{\partial \rho_{i_e}} = -\mathbf{H}_{i_{eg}}^T \mathbf{K}^{-1} \frac{\partial \mathbf{K}}{\partial \rho_{i_e}} \mathbf{U} = -\mathbf{Z}_{i_{eg}}^T \frac{\partial \mathbf{K}}{\partial \rho_{i_e}} \mathbf{U} \quad (52)$$

where $\mathbf{Z}_{i_{eg}}$ is the adjoint variable obtained by solving the following adjoint equation:

$$\mathbf{K} \mathbf{Z}_{i_{eg}} = \mathbf{H}_{i_{eg}} \quad (53)$$

The sensitivity of the output voltage can be obtained using Eq.(46), Eq.(47), Eq.(48) and Eq.(52).

The sensitivity of mean compliance in Eq.(14) is obtained as follows:

$$\frac{\partial l}{\partial \rho_{i_e}} = -\mathbf{U}^T \frac{\partial \mathbf{K}}{\partial \rho_{i_e}} \mathbf{U} \quad (54)$$

The detailed derivation of Eq.(54) can be seen in (Bendsøe and Sigmund, 2003).

3.3 Numerical Implementation for a multi-axis load cell

3.3.1 Derivation of strain compliance matrix using FEM

The strain compliance matrix \mathbf{C}_s is derived using FEM. We define the i_g -th strain gauge as being located on the i_e -th element, and formulate the discretized strain $\varepsilon_{g i_g}^h$ detected by the strain gauge as follows:

$$\begin{aligned} \varepsilon_{g i_g}^h &= \mathbf{T}_{i_g} \boldsymbol{\varepsilon}_{i_{eg}}^h = \mathbf{T}_{i_g} \mathbf{B}_{i_{eg}} \mathbf{U}_{i_{eg}} = \mathbf{T}_{i_g} \mathbf{B}_{i_{eg}} \mathbf{H}_{i_{eg}}^T \mathbf{U} \\ &= \mathbf{T}_{i_g} \mathbf{B}_{i_{eg}} \mathbf{H}_{i_{eg}}^T \mathbf{K}^{-1} \mathbf{F} = \mathbf{T}_{i_g} \mathbf{B}_{i_{eg}} \mathbf{H}_{i_{eg}}^T \mathbf{K}^{-1} \mathbf{H}_f \mathbf{f} \\ &= \mathbf{T}_{i_g} \mathbf{B}_{i_{eg}} \mathbf{Z}_{i_{eg}}^T \mathbf{H}_f \mathbf{f} = \mathbf{A}_{i_g} \mathbf{f} \end{aligned} \quad (55)$$

where

$$\begin{aligned} \boldsymbol{\varepsilon}_{i_{eg}}^h &= \mathbf{B}_{i_{eg}} \mathbf{U}_{i_{eg}}, \quad \mathbf{U}_{i_{eg}} = \mathbf{H}_{i_{eg}}^T \mathbf{U}, \quad \mathbf{F} = \mathbf{H}_f \mathbf{f}, \\ \mathbf{A}_{i_g} &= \mathbf{T}_{i_g} \mathbf{B}_{i_{eg}} \mathbf{Z}_{i_{eg}}^T \mathbf{H}_f \end{aligned} \quad (56)$$

\mathbf{H}_f is a matrix connecting the local force vector \mathbf{f} and global force vector \mathbf{F} . $\mathbf{Z}_{i_{eg}}$ is the adjoint variable obtained from Eq.(53). Using Eq.(11), Eq.(18) and

Eq.(56), the output signal vector \mathbf{s} can be obtained as follows:

$$\begin{aligned} \mathbf{s} &= \begin{pmatrix} V_{\text{out}1} \\ \vdots \\ V_{\text{out}n} \end{pmatrix} \\ &= \frac{1}{4} K_s V_{\text{in}} \begin{pmatrix} \varepsilon_{g1}^h - \varepsilon_{g2}^h + \varepsilon_{g3}^h - \varepsilon_{g4}^h \\ \vdots \\ \varepsilon_{gn_g-3}^h - \varepsilon_{gn_g-2}^h + \varepsilon_{gn_g-1}^h - \varepsilon_{gn_g}^h \end{pmatrix} \\ &= \frac{1}{4} K_s V_{\text{in}} \begin{pmatrix} \mathbf{A}_1 - \mathbf{A}_2 + \mathbf{A}_3 - \mathbf{A}_4 \\ \vdots \\ \mathbf{A}_{n_g-3} - \mathbf{A}_{n_g-2} + \mathbf{A}_{n_g-1} - \mathbf{A}_{n_g} \end{pmatrix} \mathbf{f} \end{aligned} \quad (57)$$

Comparing Eq.(17) and Eq.(57), matrix \mathbf{C}_s can be obtained as follows:

$$\mathbf{C}_s = \frac{1}{4} K_s V_{\text{in}} \begin{pmatrix} \mathbf{A}_1 - \mathbf{A}_2 + \mathbf{A}_3 - \mathbf{A}_4 \\ \vdots \\ \mathbf{A}_{n_g-3} - \mathbf{A}_{n_g-2} + \mathbf{A}_{n_g-1} - \mathbf{A}_{n_g} \end{pmatrix} \quad (58)$$

3.3.2 Sensitivity analysis

The sensitivity of the singular value of \mathbf{C}_s , the objective function for a multi-axis load cell is derived as follows. Let $\sigma_j(\mathbf{C}_s)$ and $\lambda_j(\mathbf{C}_s)$ denote the j -th singular value and j -th eigenvalue of \mathbf{C}_s respectively. The following relationship exists between singular values and eigenvalues (Golub and Van Loan, 1996):

$$\sigma_j(\mathbf{C}_s) = \sqrt{\lambda_j(\mathbf{C}_s^T \mathbf{C}_s)} \quad (59)$$

That is, the sensitivity of the j -th singular value with respect to the density function ρ_{i_e} is obtained as follows using the sensitivity of the j -th eigenvalue:

$$\frac{\partial \sigma_j(\mathbf{C}_s)}{\partial \rho_{i_e}} = \frac{1}{\sqrt{\lambda_j(\mathbf{C}_s^T \mathbf{C}_s)}} \frac{\partial \lambda_j(\mathbf{C}_s^T \mathbf{C}_s)}{\partial \rho_{i_e}} \quad (60)$$

The sensitivity of $\lambda_j(\mathbf{C}_s^T \mathbf{C}_s)$ with respect to ρ_{i_e} is obtained as follows (Haug et al., 1986):

$$\begin{aligned} \frac{\partial \lambda_j(\mathbf{C}_s^T \mathbf{C}_s)}{\partial \rho_{i_e}} &= \phi_j^T \frac{\partial (\mathbf{C}_s^T \mathbf{C}_s)}{\partial \rho_{i_e}} \phi_j \\ &= \phi_j^T \left(\frac{\partial \mathbf{C}_s^T}{\partial \rho_{i_e}} \mathbf{C}_s + \mathbf{C}_s^T \frac{\partial \mathbf{C}_s}{\partial \rho_{i_e}} \right) \phi_j \end{aligned} \quad (61)$$

where ϕ_j is normalized j -th eigenvector.

If the above j -th eigenvalue is a repeated eigenvalue, this sensitivity cannot be used, since repeated eigenvalues have only directional derivatives. In this case, the sensitivities are obtained as results from the following eigenvalue problem (Haug et al., 1986; Seyranian et al., 1994; Ohsaki and Ikeda, 2007).

$$\mathbf{M}\mathbf{a} = \frac{\partial \lambda_j (\mathbf{C}_s^T \mathbf{C}_s)}{\partial \rho_{i_e}} \mathbf{a}, \quad \mathbf{M} \in \mathbb{R}^{s \times s}, \quad \mathbf{a} \in \mathbb{R}^s \quad (62)$$

where

$$M_{ij} = \phi_i^T \left(\frac{\partial \mathbf{C}_s^T}{\partial \rho_{i_e}} \mathbf{C}_s + \mathbf{C}_s^T \frac{\partial \mathbf{C}_s}{\partial \rho_{i_e}} \right) \phi_j, \quad i, j = 1, \dots, s \quad (63)$$

where s is the number of repeated eigenvalues, \mathbf{M} is the $s \times s$ matrix whose components are represented by Eq.(63), and \mathbf{a} is the s -dimensional eigenvector representing the derivative directions.

We calculate $\partial \mathbf{C}_s / \partial \rho_{i_e}$ using Eq.(58), as follows:

$$\frac{\partial \mathbf{C}_s}{\partial \rho_{i_e}} = \frac{1}{4} K_s V_{in} \begin{pmatrix} \frac{\partial \mathbf{A}_1}{\partial \rho_{i_e}} - \frac{\partial \mathbf{A}_2}{\partial \rho_{i_e}} + \frac{\partial \mathbf{A}_3}{\partial \rho_{i_e}} - \frac{\partial \mathbf{A}_4}{\partial \rho_{i_e}} \\ \vdots \\ \frac{\partial \mathbf{A}_{n_g-3}}{\partial \rho_{i_e}} - \frac{\partial \mathbf{A}_{n_g-2}}{\partial \rho_{i_e}} + \frac{\partial \mathbf{A}_{n_g-1}}{\partial \rho_{i_e}} - \frac{\partial \mathbf{A}_{n_g}}{\partial \rho_{i_e}} \end{pmatrix} \quad (64)$$

We now calculate $\partial \mathbf{A}_{i_g} / \partial \rho_{i_e}$. Using Eq.(55), the following equation is obtained,

$$\mathbf{A}_{i_g} \mathbf{f} = \mathbf{T}_{i_g} \mathbf{B}_{i_{eg}} \mathbf{H}_{i_{eg}}^T \mathbf{U} \quad (65)$$

Taking a derivative of both sides with respect to ρ_{i_e} :

$$\frac{\partial \mathbf{A}_{i_g} \mathbf{f}}{\partial \rho_{i_e}} = \mathbf{T}_{i_g} \mathbf{B}_{i_{eg}} \mathbf{H}_{i_{eg}}^T \frac{\partial \mathbf{U}}{\partial \rho_{i_e}} \quad (66)$$

Substituting Eq.(51) into Eq.(66), the following equation can be obtained:

$$\begin{aligned} \frac{\partial \mathbf{A}_{i_g} \mathbf{f}}{\partial \rho_{i_e}} &= -\mathbf{T}_{i_g} \mathbf{B}_{i_{eg}} \mathbf{H}_{i_{eg}}^T \mathbf{K}^{-1} \frac{\partial \mathbf{K}}{\partial \rho_{i_e}} \mathbf{U} \\ &= -\mathbf{T}_{i_g} \mathbf{B}_{i_{eg}} \mathbf{Z}_{i_{eg}}^T \frac{\partial \mathbf{K}}{\partial \rho_{i_e}} \mathbf{U} \\ &= -\mathbf{T}_{i_g} \mathbf{B}_{i_{eg}} \mathbf{Z}_{i_{eg}}^T \frac{\partial \mathbf{K}}{\partial \rho_{i_e}} \mathbf{K}^{-1} \mathbf{F} \\ &= -\mathbf{T}_{i_g} \mathbf{B}_{i_{eg}} \mathbf{Z}_{i_{eg}}^T \frac{\partial \mathbf{K}}{\partial \rho_{i_e}} \mathbf{K}^{-1} \mathbf{H}_f \mathbf{f} \\ &= -\mathbf{T}_{i_g} \mathbf{B}_{i_{eg}} \mathbf{Z}_{i_{eg}}^T \frac{\partial \mathbf{K}}{\partial \rho_{i_e}} \mathbf{Z}_f \mathbf{f} \end{aligned} \quad (67)$$

where \mathbf{Z}_f is an adjoint variable obtained by solving the following adjoint equation:

$$\mathbf{K} \mathbf{Z}_f = \mathbf{H}_f \quad (68)$$

The following equation can be derived:

$$\frac{\partial \mathbf{A}_{i_g}}{\partial \rho_{i_e}} = -\mathbf{T}_{i_g} \mathbf{B}_{i_{eg}} \mathbf{Z}_{i_{eg}}^T \frac{\partial \mathbf{K}}{\partial \rho_{i_e}} \mathbf{Z}_f \quad (69)$$

Using Eq.(60), Eq.(61), Eq.(64) and Eq.(69) the sensitivity of a singular value with respect to a design variable can be obtained.

4 Numerical examples

We present the simple 2D numerical examples to confirm the utility of the proposed method. The structural material is assumed to be aluminum. We assume the strain gauges have an axial length small enough to fit each finite element, and the gauge factor K_s is 2.1. The input voltage of the Wheatstone bridges is set to 24V. All strain gauges are located on the centers of the finite elements, and 3×3 elements around the positions of the strain gauges are regarded as non-design and fully dense elements. The finite elements are formulated as 4-node isoparametric elements. The upper bound of the volume constraint V^U is set as 40% of the entire volume. The minimum value of the density function is set to 10^{-3} . As shown in Eq.(40) and Eq.(41), we solve the multi-objective optimization problem composed of objective functions whose values are different orders of magnitude. Thus, to streamline the setting of the weighting coefficients, we normalize each objective function using its initial value.

4.1 Optimization of a single-axis load cell

The first example is the optimization of a single-axis load cell. Figure 3 shows the design domain. The domain is discretized into a 100×50 square mesh. From 1 to 4 strain gauges are located on the points (i)-(iv) shown in Fig.3. The left side of the domain is fixed and the measured load is assumed to be a vertical load on the center of the right side. Weighting coefficients of Eq.(15) are set to the following three patterns: ($w_V = 0.1, w_l = 0.9$), ($w_V = 0.2, w_l = 0.8$), ($w_V = 0.3, w_l = 0.7$). To obtain structures with a certain level of stiffness, the weighting coefficients used for the mean compliances are larger in value than any one used for the output voltages. We perform 200 optimization iterations. β in Eq.(6) is set to 1 for the first 100 iterations. To obtain solutions that most closely approach values of 0 and 1, β is raised by 1 every 5 iterations beyond the first 100 iterations. The scale parameter r_{\min} in Eq.(4) is set to 3.

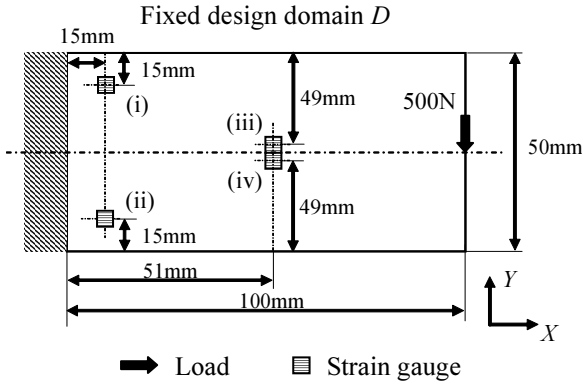


Fig. 3 Design domain for example 1

Figure 4 shows the optimal configuration with one strain gauge on position (i). Figure 5 shows the optimal configuration with two strain gauges on positions (i) and (ii) respectively. Figure 6 shows the optimal configuration with four strain gauges on positions (i) to (iv). In each figure, (a),(b) and (c) show the optimal configurations after 100 iterations and (d),(e) and (f) show the optimal configurations after 200 iterations. Table 1 shows the angle of each strain gauge θ , resistance variation ΔR , the output voltage in Eq.(15) V_{out} , and the compliance l . The angle θ means the angle between the local coordinate systems of strain gauges and the global coordinate system shown in Fig.1. Figure 7 shows the history of the output voltage for each case.

Figure 7 confirms that the output voltage increased in each case during the optimization process until 100 iterations were completed. After that, the output voltage decreased gradually with the increase in the penalization parameter β of the Heaviside step projection function depend on the conditions. In the case of one strain gauge, from the optimal values of V_{out} and Fig.4, as w_V becomes large, we found the position of the lower support bar on the left side moved to the upper side and the strain at the strain gauge point increased. In the case using two strain gauges, we found similar shapes with two horizontal pillars at the location of the strain gauges, and a typical cantilever-like structure as shown in Fig.5. It is postulated that the mechanism responsible for the structure involves transmission of the load to the strain gauges at the left pillar-like structure due to the high stiffness of the structure, and the high strain is detected by these strain gauges. As shown in Fig.6, in the structure with 4 strain gauges, high strain seems to occur in the connecting element between the lower structure and the upper structure. The almost symmetric structures and location angles of the strain gauges shown in Table 1 were obtained in the case of two and four strain gauges. Thus, the sensors in each

half domain are sensing the tension and compression strains. From Table 1, we find that a larger number of strain gauges does not always yield a higher voltage. We noted that the higher output voltage was obtained in a 1-strain gauge case with $(w_V = 0.3, w_l = 0.7)$ compared with the 2-strain gauge cases. This could be due to the dependency on initial setting in the optimization problem here, which is to maximize the absolute value of local strain based on the sensitivity analysis and the gradient method. That is, since the optimization process must maximize all the local strains at the strain gauge location, it is hard to obtain a solution that ignores some of these strain gauges. In the examples with one and two strain gauges, the best results in terms of the voltage are shown in Fig.4(f), which are closer to global optima. Such a shape could not be obtained if two strain gauges were located at the specified point because our method cannot ignore the lower strain gauge. However, since the optimization problem is a multi-objective optimization problem covering stiffness and voltage the highest voltage in not always the best solution. Comparing Fig.4(f) with Fig.5(f), Fig.5(f) is clearly a stiffer structure.

4.2 Optimization of a multi-axis load cell

The simple 2D numerical example is also presented for the optimization of a multi-axis load cell structure. The design domain is illustrated in Fig.8. The domain is discretized into a 50×100 square mesh. We set the following two patterns of strain gauge locations. In Case A, strain gauge No.1 is located at position (i) and No.2 is located at position (ii). In Case B, strain gauge No.1 is located at position (iii) and No.2 is located at position (iv). The two Wheatstone bridges are constructed using strain gauge No.1 and strain gauge No.2 and referred to as Wheatstone bridge No.1 and Wheatstone bridge No.2. The output voltages in the output signal vectors V_{out1} and V_{out2} in Eq.(17) correspond to the output voltages of Wheatstone bridge No.1 and No.2 respectively. The load point is located at the center of the right side of the domain. To calculate the mean compliance for the optimization of stiffness, two types of load cases are considered. The loads are used to decide the angle of the strain gauges. The directions of strain gauge No.1 and 2 are set to the directions of the principal strain that caused load case 1 and load case 2. The volume constraint is set to 40% of the full volume of the domain. The weighting coefficients in Eq.(41) are set to the following two patterns, $(w_s = 0.3, w_c = 0.3, w_{l1} = 0.2, w_{l2} = 0.2)$ and $(w_s = 0.4, w_c = 0.4, w_{l1} = 0.1, w_{l2} = 0.1)$. We perform 300 optimization iterations. β in Eq.(6) is set to 1 for

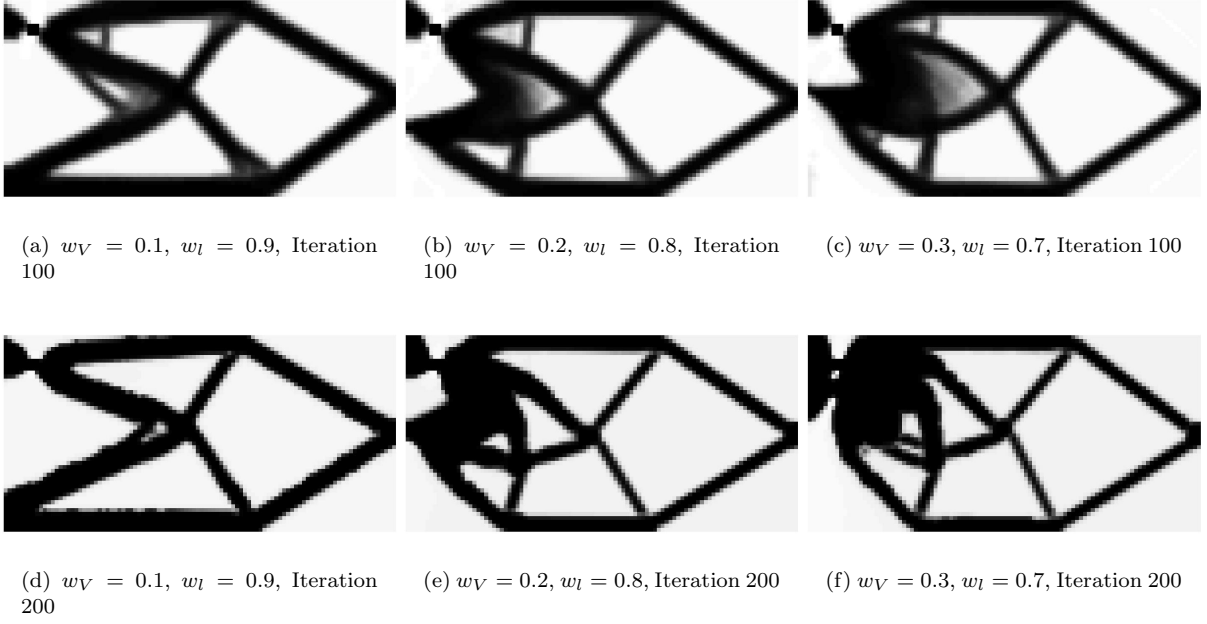


Fig. 4 Optimal configuration of example 1 (1 strain gauge)

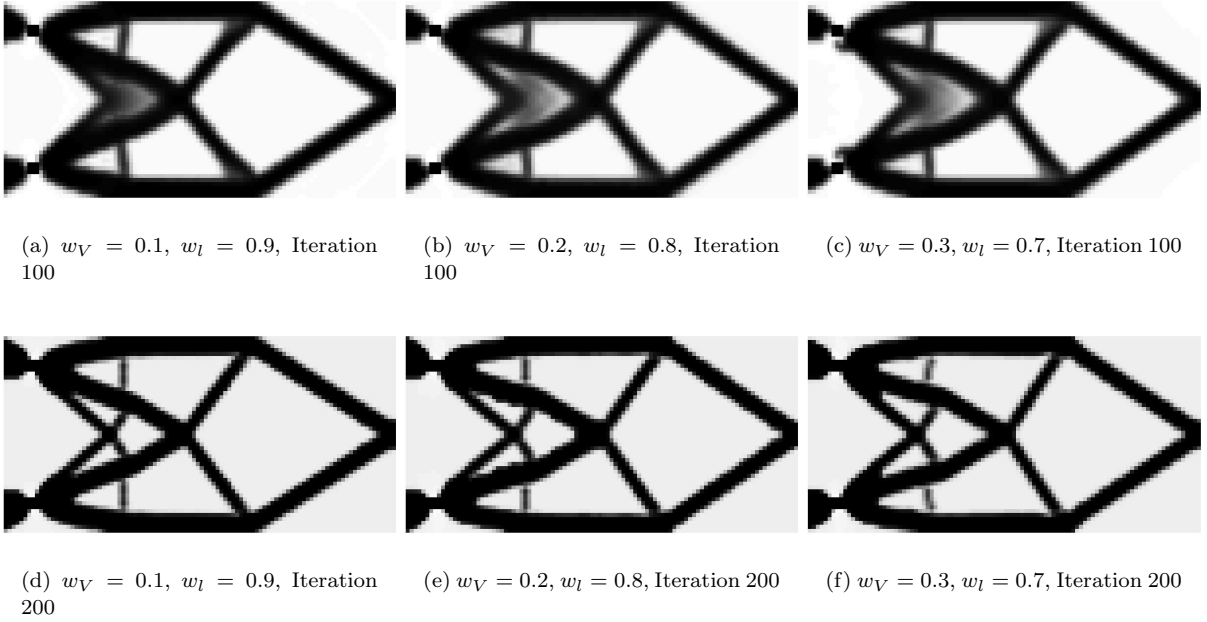


Fig. 5 Optimal configuration of example 1 (2 strain gauges)

the first 200 iterations. To obtain a shape that most clearly represents 0 and 1 values, β is incremented by 1 after every 5 iterations. The scale parameter r_{\min} in Eq.(4) is set to 3.

Figures 9 and 10 show the optimal configurations for each strain gauge location obtained by each of the weighting patterns. In each figure, (a) and (b) show the optimal configurations after 200 iterations and (c) and

(d) show the optimal configurations after 300 iterations. Table 2 presents the initial and optimal values of the two lowest singular values, σ_1 , σ_2 ; the condition number, σ_1/σ_2 ; the angle of strain gauges on the optimal structure, θ ; the mean compliances for each load case, l^1 and l^2 ; the resistance variation in the i -th strain gauge for the load case j , ΔR_i^j ; and the output voltage of the i -th Wheatstone bridge for the load case j , V_i^j . Figure

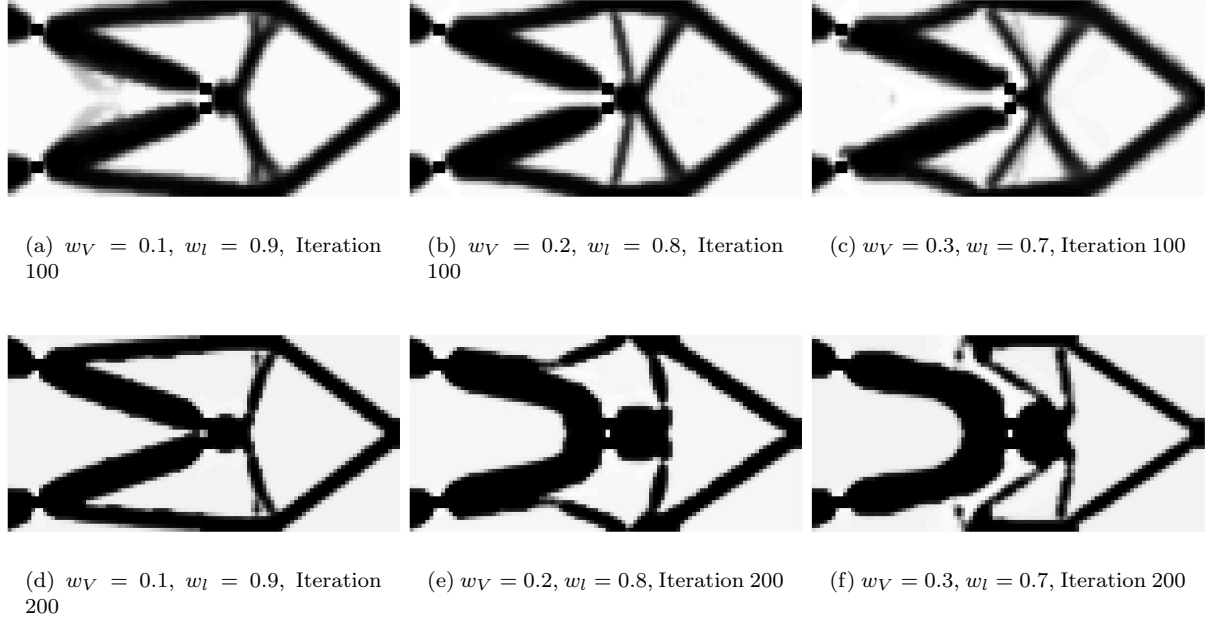


Fig. 6 Optimal configuration of example 1 (4 strain gauges)

Table 1 Optimal results for example 1

(a) 1 strain gauge											
w_V	w_I	$\theta_1(^{\circ})$	$\theta_2(^{\circ})$	$\theta_3(^{\circ})$	$\theta_4(^{\circ})$	$\Delta R_1 (\Omega)$	$\Delta R_2 (\Omega)$	$\Delta R_3 (\Omega)$	$\Delta R_4 (\Omega)$	$V_{\text{out}} (\text{V})$	$I (\text{J})$
0.1	0.9	-3.98	-	-	-	6.58×10^{-4}	-	-	-	3.94×10^{-3}	4.03×10^{-2}
0.2	0.8	-10.01	-	-	-	1.33×10^{-3}	-	-	-	7.97×10^{-3}	1.00×10^{-1}
0.3	0.7	-5.00	-	-	-	2.81×10^{-3}	-	-	-	1.69×10^{-2}	3.89×10^{-1}
(b) 2 strain gauges											
w_V	w_I	$\theta_1(^{\circ})$	$\theta_2(^{\circ})$	$\theta_3(^{\circ})$	$\theta_4(^{\circ})$	$\Delta R_1 (\Omega)$	$\Delta R_2 (\Omega)$	$\Delta R_3 (\Omega)$	$\Delta R_4 (\Omega)$	$V_{\text{out}} (\text{V})$	$I (\text{J})$
0.1	0.9	-5.70	5.70	-	-	6.33×10^{-4}	-6.33×10^{-4}	-	-	7.62×10^{-3}	4.78×10^{-2}
0.2	0.8	-6.23	6.23	-	-	6.96×10^{-4}	-6.96×10^{-4}	-	-	8.35×10^{-3}	4.90×10^{-2}
0.3	0.7	-6.35	6.35	-	-	7.08×10^{-4}	-7.08×10^{-4}	-	-	8.49×10^{-3}	4.99×10^{-2}
(c) 4 strain gauges											
w_V	w_I	$\theta_1(^{\circ})$	$\theta_2(^{\circ})$	$\theta_3(^{\circ})$	$\theta_4(^{\circ})$	$\Delta R_1 (\Omega)$	$\Delta R_2 (\Omega)$	$\Delta R_3 (\Omega)$	$\Delta R_4 (\Omega)$	$V_{\text{out}} (\text{V})$	$I (\text{J})$
0.1	0.9	-6.30	6.70	-10.54	10.53	6.00×10^{-4}	-6.00×10^{-4}	4.29×10^{-4}	-4.29×10^{-4}	1.23×10^{-2}	5.43×10^{-2}
0.2	0.8	-6.02	6.02	-6.87	6.87	6.83×10^{-4}	-6.83×10^{-4}	9.00×10^{-4}	-9.00×10^{-4}	1.91×10^{-2}	9.13×10^{-2}
0.3	0.7	-5.66	5.66	-6.07	6.07	7.00×10^{-4}	-7.00×10^{-4}	1.23×10^{-3}	-1.23×10^{-3}	2.33×10^{-2}	1.58×10^{-1}

11 illustrates the history of Euclidean norm of the output signal vector \mathbf{S} . The strain compliance matrices \mathbf{C}_s of each optimal configuration are expressed in Eq.(70) and Eq.(71):

$$\begin{aligned} \mathbf{C}_s(\text{case A}, w_s = 0.3, w_c = 0.3, w_{l1} = 0.2, w_{l2} = 0.2) \\ = \begin{pmatrix} 2.56 & 0.77 \\ -0.74 & 2.76 \end{pmatrix} \times 10^{-6} \end{aligned} \quad (70)$$

$$\begin{aligned} \mathbf{C}_s(\text{case A}, w_s = 0.4, w_c = 0.4, w_{l1} = 0.1, w_{l2} = 0.1) \\ = \begin{pmatrix} 4.26 & 0.66 \\ 0.68 & -4.17 \end{pmatrix} \times 10^{-6} \end{aligned} \quad (71)$$

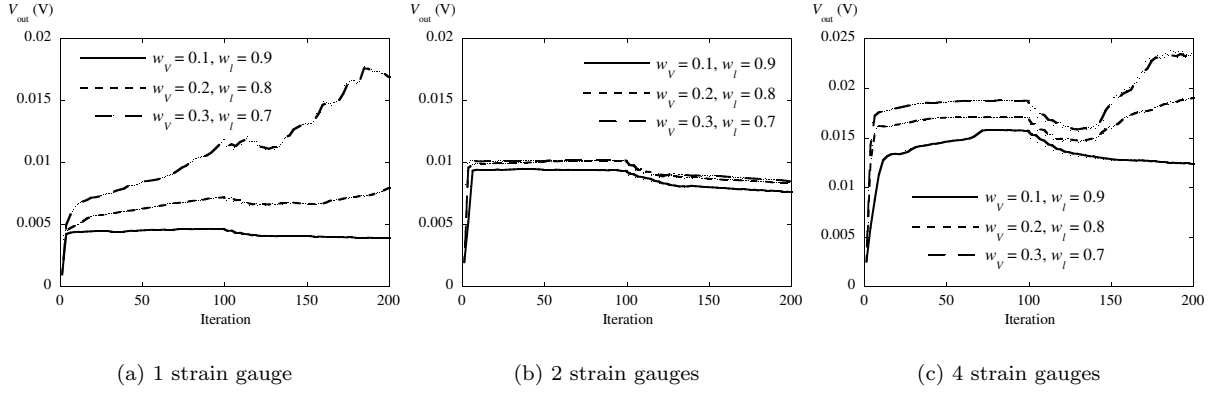


Fig. 7 History of output voltage of example 1

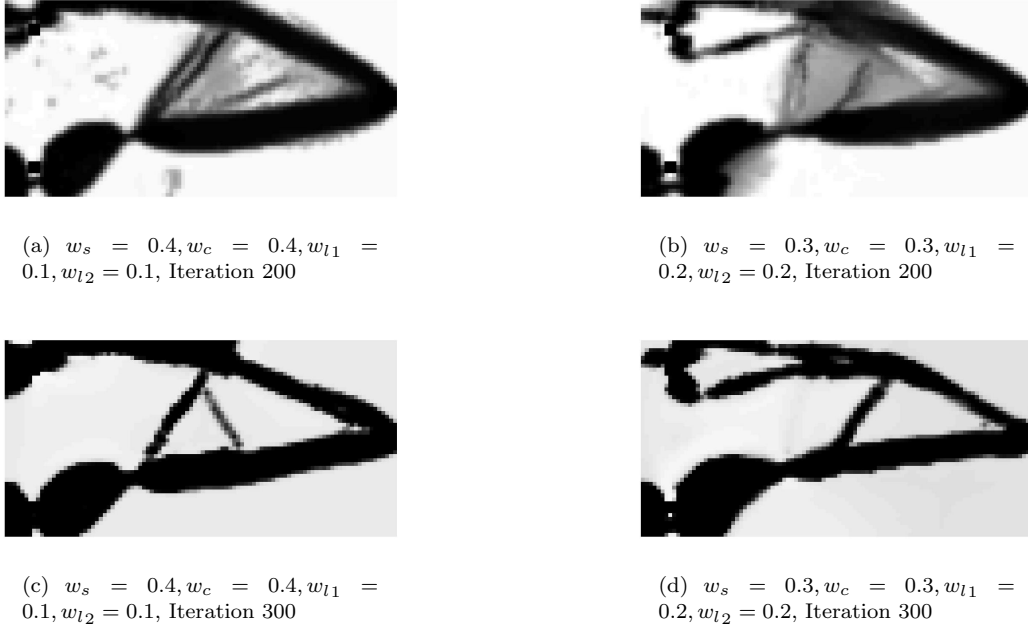


Fig. 9 Optimal configurations for case A of example 2

$$\begin{aligned}
 C_s(\text{case B}, w_s = 0.3, w_c = 0.3, w_{l1} = 0.2, w_{l2} = 0.2) \\
 = \begin{pmatrix} 4.72 & 5.55 \\ 4.94 & -5.33 \end{pmatrix} \times 10^{-6}
 \end{aligned} \tag{72}$$

$$\begin{aligned}
 C_s(\text{case B}, w_s = 0.4, w_c = 0.4, w_{l1} = 0.1, w_{l2} = 0.1) \\
 = \begin{pmatrix} 4.49 & 8.38 \\ 7.68 & -4.56 \end{pmatrix} \times 10^{-6}
 \end{aligned} \tag{73}$$

Figures 9 and 10 indicate that clear configurations are obtained using our method. Table 2 indicates that the singular values, σ_1/σ_2 , of the optimal configurations have a nearly ideal value of 1, and these structures demonstrate an almost ideal detection accuracy for each

force component. Table 2 and Fig.11 reveals that the sensitivity of force detection can be increased using our method, however, output voltages decreased during the penalization process used to mitigate gray areas. Moreover, oscillations are observed in the locations of the strain gauges in Case B. The reason for this is unclear, but the solutions finally converge and reasonable shapes are obtained. Higher weighting coefficients, w_s and w_c , yield a more sensitive structure. On the other hand, the optimal configurations have almost equal output voltages for each load case. Thus, the error in the strain detection can affect both X and Y load directions equally. Of particular interest is that more sensitive optimal results are obtained by the more ‘‘challenging’’

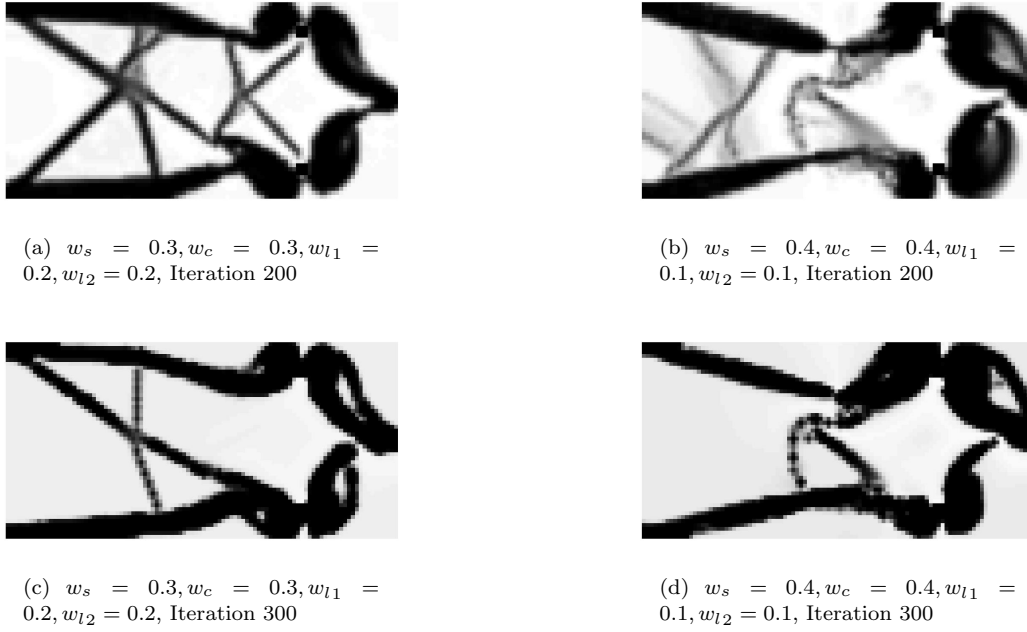


Fig. 10 Optimal configurations for case B of example 2

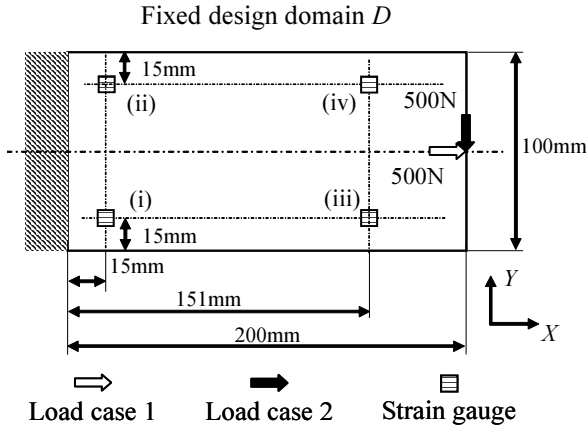


Fig. 8 Design domain for example 2

strain gauge location in Case B. However, in terms of stiffness, the optimal structures in Case A are better than those one in by Case B. Thus, we obtain a variety of configurations .

5 Conclusion

In this paper, we developed a structural topology optimization method for single- and multi-axis load cell structures and achieved the following:

1. The topology optimization method was implemented using the SIMP method and the projection method.

2. The sensitivity of force detection is formulated as a design requirement of the single-axis load cell.
3. The design requirements of the multi-axis load cell were defined as follows; 1: the rank of C_s , 2: the sensitivity, and 3: the detection accuracy of each force component and its evaluation method as formulated on the basis of SVD.
4. An objective function was formulated to help meet the above design requirement.
5. The sensitivity of the objective function was calculated. In particular, the sensitivity of the singular value was formulated based on the existing formulation of eigenvalue sensitivity, and an optimization algorithm was constructed using FEM and MMA.
6. Simple 2D examples established the usefulness of our proposed methodology for the optimization of single- and multi-axis load cell structures.

In future research, we intend to extend our method to problems considering the optimal location of strain gauges, to obtain higher performance, and to solve three dimensional design problems.

Acknowledgements This work was partly supported by the JGC-S scholarship foundation, the MAZAK foundation and CNPq (Conselho Nacional de Desenvolvimento Científico e Tecnológico-Brazilian National Council for Scientific and Technological Development). We are deeply grateful to Prof. Svanberg for providing the source code for the Method of Moving Asymptotes (MMA).

Table 2 Initial values and optimal results

				(a) Case A								
Initial values				σ_1	σ_2	σ_1/σ_2						
				2.78×10^{-6}	3.64×10^{-7}	7.64						
w_s	w_c	w_{l1}	w_{l2}	σ_1	σ_2	σ_1/σ_2	l_1 (J)	l_2 (J)	θ_1 (°)	θ_2 (°)		
0.3	0.3	0.2	0.2	2.87×10^{-6}	2.66×10^{-6}	1.08	6.27	60.13	1.64	29.61		
0.4	0.4	0.1	0.1	4.31×10^{-6}	4.22×10^{-6}	1.02	10.04	84.94	1.46	-78.22		
w_s	w_c	w_{l1}	w_{l2}	ΔR_1^1 (Ω)	ΔR_2^1 (Ω)	ΔR_1^2 (Ω)	ΔR_2^2 (Ω)	V_{out11} (V)	V_{out12} (V)	V_{out21} (V)	V_{out22} (V)	
0.3	0.3	0.2	0.2	2.13×10^{-4}	-6.16×10^{-5}	-6.39×10^{-5}	-2.31×10^{-4}	1.28×10^{-3}	3.69×10^{-4}	3.83×10^{-4}	1.39×10^{-3}	
0.4	0.4	0.1	0.1	3.55×10^{-4}	5.64×10^{-5}	-5.50×10^{-5}	3.47×10^{-4}	2.13×10^{-3}	3.38×10^{-4}	3.30×10^{-4}	2.08×10^{-3}	
				(b) Case B								
Initial values				σ_1	σ_2	σ_1/σ_2						
				8.71×10^{-7}	3.03×10^{-7}	2.88						
w_s	w_c	w_{l1}	w_{l2}	σ_1	σ_2	σ_1/σ_2	l_1 (J)	l_2 (J)	θ_1 (°)	θ_2 (°)		
0.3	0.3	0.2	0.2	7.33×10^{-6}	6.62×10^{-6}	1.11	19.39	80.35	6.57	-4.84		
0.4	0.4	0.1	0.1	9.57×10^{-6}	8.87×10^{-6}	1.08	29.08	123.27	7.93	-6.99		
w_s	w_c	w_{l1}	w_{l2}	ΔR_1^1 (Ω)	ΔR_2^1 (Ω)	ΔR_1^2 (Ω)	ΔR_2^2 (Ω)	V_{out11} (V)	V_{out12} (V)	V_{out21} (V)	V_{out22} (V)	
0.3	0.3	0.2	0.2	3.94×10^{-4}	4.12×10^{-4}	-4.63×10^{-4}	4.44×10^{-4}	2.36×10^{-3}	2.47×10^{-3}	2.78×10^{-3}	2.66×10^{-3}	
0.4	0.4	0.1	0.1	3.74×10^{-4}	6.40×10^{-4}	-6.99×10^{-4}	3.80×10^{-4}	2.25×10^{-3}	3.84×10^{-3}	4.19×10^{-3}	2.28×10^{-3}	

References

- G. Allaire. *Shape Optimization by the Homogenization Method*. Springer-Verlag, New York, 2001.
- E. Bayo and J. R. Stubbe. Six-axis force sensor evaluation and a new type of optimal frame truss design for robotic applications. *J. Robot. Syst.*, 6(2):191–208, 1989.
- M. P. Bendsøe. Optimal shape design as a material distribution problem. *Struct. Optim.*, 1(4):193–202, 1989.
- M. P. Bendsøe and N. Kikuchi. Generating optimal topologies in structural design using a homogenization method. *Comput. Meth. Appl. Mech. Eng.*, 71(2):197–224, 1988.
- M. P. Bendsøe and O. Sigmund. Material interpolation schemes in topology optimization. *Arch. Appl. Mech.*, 69(9):635–654, 1999.
- M. P. Bendsøe and O. Sigmund. *Topology Optimization: Theory, Methods, and Applications*. Springer-Verlag, Berlin, 2003.
- S. Canfield and M. Frecker. Topology optimization of compliant mechanical amplifiers for piezoelectric actuators. *Struct. Multidisc. Optim.*, 20(4):269–279, 2000.

- L. P. Chao and K. T. Chen. Shape optimal design and force sensitivity evaluation of six-axis force sensors. *Sensor. Actuator. Phys.*, 63(2):105–112, 1997.
- A. Diaz and O. Sigmund. Checkerboard patterns in layout optimization. *Struct. Optim.*, 10(1):40–45, 1995.
- G.H. Golub and C.F. Van Loan. *Matrix Computations (3rd Edition)*. The Johns Hopkins University Press, 1996.
- J. K. Guest, J. H. Prévost, and T. Belytschko. Achieving minimum length scale in topology optimization using nodal design variables and projection functions. *Int. J. Numer. Meth. Eng.*, 61(2):238–254, 2004.
- E. J. Haug, K. K. Choi, and V. Komkov. *Design Sensitivity Analysis of Structural Systems*. Academic Press, Orlando, FL, 1986.
- M. Kaneko. Twin-head six-axis force sensors. *IEEE Trans. Robot. Autom.*, 12(1):146–154, 1996.
- G.S. Kim and H.D. Lee. Development of a six-axis force/moment sensor and its control system for an intelligent robot's gripper. *Meas. Sci. Tech.*, 14:1265–1274, 2003.
- J. A. Kim, E. W. Bae, S. H. Kim, and Y. K. Kwak. Design methods for six-degree-of-freedom displacement measurement systems using cooperative targets. *Precis. Eng.*, 26:99–104, 2002.

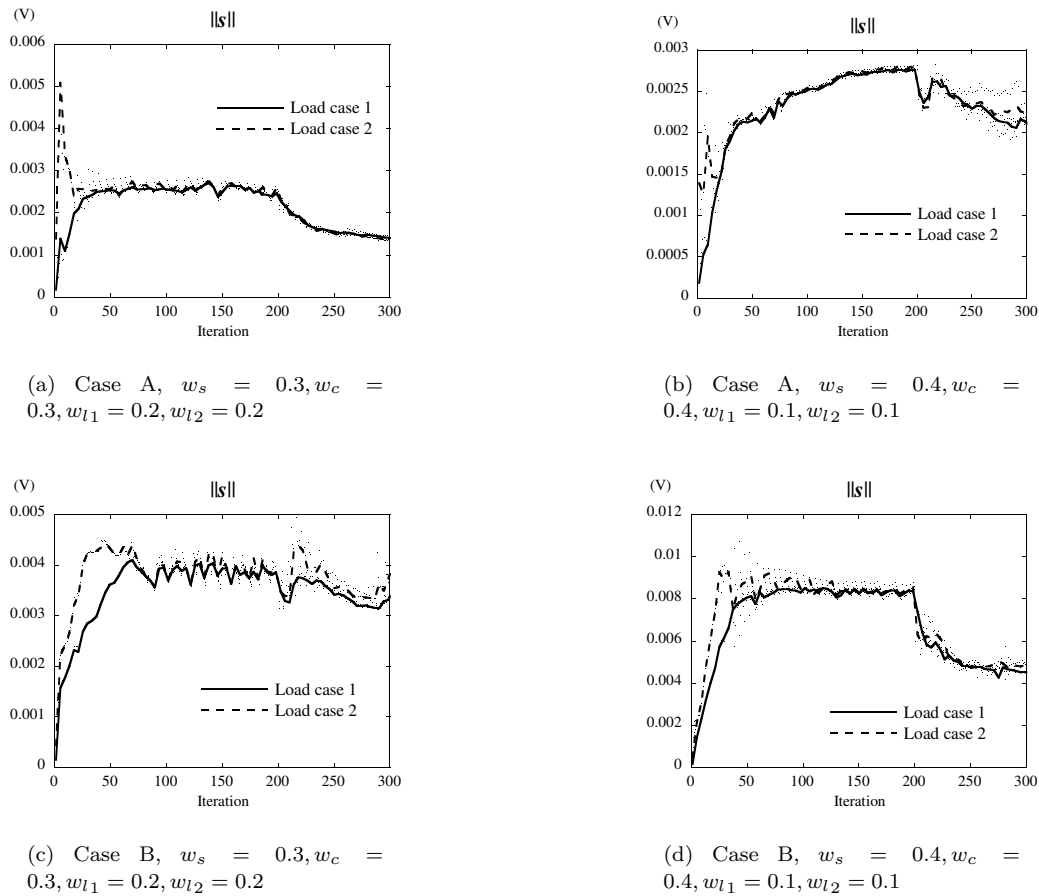


Fig. 11 History of output signals (Euclidean norm)

L.A. Krog and N. Olhoff. Optimum topology and reinforcement design of disk and plate structures with multiple stiffness and eigenfrequency objectives. *Comput. Struct.*, 72(4-5):535–563, 1999.

S. A. Liu and H. L. Tzo. A novel six-component force sensor of good measurement isotropy and sensitivities. *Sensor. Actuator. Phys.*, 100(2-3):223–230, 2002.

Z. D. Ma, N. Kikuchi, and H. C. Cheng. Topological design for vibrating structures. *Comput. Meth. Appl. Mech. Eng.*, 121(1-4):259–280, 1995.

K. Matsui and K. Terada. Continuous approximation of material distribution for topology optimization. *Int. J. Numer. Meth. Eng.*, 59:1925–1944, 2004.

S. Nishiwaki, M.I. Frecker, S. Min, and N. Kikuchi. Topology optimization of compliant mechanisms using the homogenization method. *Int. J. Numer. Meth. Eng.*, 42:535–559, 1998.

M. Ohsaki and K. Ikeda. *Stability and Optimization of Structures: Generalized Sensitivity Analysis*. Springer, 2007.

J.J. Park and G.S. Kim. Development of the 6-axis force/moment sensor for an intelligent robot’s gripper. *Sensor. Actuator. Phys.*, 118(1):127–134, 2005.

C. B. W. Pedersen. Crashworthiness design of transient frame structures using topology optimization. *Comput. Meth. Appl. Mech. Eng.*, 193(6-8):653–678, 2004.

N. L. Pedersen. Maximization of eigenvalues using topology optimization. *Struct. Multidisciplinary Optim.*, 20(1):2–11, 2000.

W. M. Rubio, E. C. N. Silva, and S. Nishiwaki. Piezoresistive sensor design using topology optimization. *Struct. Multidisc. Optim.*, 36(6):571–583, 2008.

A. P. Seyranian, E. Lund, and N. Olhoff. Multiple eigenvalues in structural optimization problems. *Struct. Optim.*, 8(4):207–227, 1994.

O. Sigmund. On the design of compliant mechanisms using topology optimization. *Mech. Struct. Mach.*, 25(4):493–524, 1997.

O. Sigmund. Design of multiphysics actuators using topology optimization—part i: one-material structures. *Comput. Meth. Appl. Mech. Eng.*, 190(49-50):

-
- 6577–6604, 2001.
- O. Sigmund. Morphology-based black and white filters for topology optimization. *Struct. Multidisc. Optim.*, 33(4):401–424, 2007.
- O. Sigmund and J. Petersson. Numerical instabilities in topology optimization: a survey on procedures dealing with checkerboards, mesh-dependencies and local minima. *Struct. Optim.*, 16(1):68–75, 1998.
- E. C. N. Silva, S. Nishiwaki, and N. Kikuchi. Topology optimization design of flextensional actuators. *IEEE Trans. Ultrason. Ferroelectrics. Freq. Contr.*, 47(3):657–671, 2000.
- K. Suzuki and N. Kikuchi. A homogenization method for shape and topology optimization. *Comput. Meth. Appl. Mech. Eng.*, 93(3):291–318, 1991.
- K. Svanberg. The method of moving asymptotes- a new method for structural optimization. *Int. J. Numer. Meth. Eng.*, 24(2):359–373, 1987.
- M. Uchiyama, E. Bayo, and E. Palma-Villalon. A systematic design procedure to minimize a performance index for robot force sensors. *J. Dyn. Syst. Meas. Contr.*, 113:388–394, 1991a.
- M. Uchiyama, Y. Nakamura, and K. Hakomori. Evaluation of the robot force sensor structure using singular value decomposition. *Adv. Robot.*, 5(1):39–52, 1991b.
- W. Weiblen and T. Hofmann. Evaluation of different designs of wheel force transducers. *SAE paper*, (980262):1–10, 1998.
- M. Zhou and G. I. N. Rozvany. The coc algorithm. ii: Topological, geometrical and generalized shape optimization. *Comput. Meth. Appl. Mech. Eng.*, 89(1-3):309–336, 1991.